Design of Rectangular Slotted-Patch Antenna Array-Sensor for Breast-Tumor Detection

Divya Chaturvedi, *Senior Member, IEEE*, V. L. Bhavani Maddirala, *Student Member, IEEE,* and Arvind Kumar, *Senior Member, IEEE*

***Abstract*— In this work, a slotted rectangular microstrip patch antenna-array-sensor is proposed for breast tumor detection operating in Industrial Scientific and Medical (ISM) frequency band at 5.8 GHz. To increase the sensitivity and better coverage region, a 1×4 antenna-array with overall size 0.96 λ_g × 2.5 λ_g has been developed instead of a single element. To excite each antenna element, a 1:4 power divider is employed in corporate feeding with microstrip technology. To acquire the conforming ability on hemispherical surface, the antenna array sensor is realized on RT Duroid 5880 of thickness 0.508 mm. A monostatic radar-based technique using microwave signals is used to detect the contrast between healthy and malignant tissues. Initially, the sensor's performance has been evaluated over a multi-layered breast equivalent phantom comprising skin and fat layers along with tumor. Specific Absorption Rate (SAR) analysis is conducted to assess the variations in the biological tissues of the breast equivalent phantom, distinguishing between healthy and malignant tissues. Also, experimental results reveal that the 1×4 array sensor provides improved sensitivity, gain, and directional energy delivery, enabling better detection of tumors at varying sizes and depths.**

Link to graphical and video abstracts, and to code: https://latamt.ieeer9.org/index.php/transactions/article/view/9775

***Index Terms*— Breast tumor diagnosis, breast phantoms, healthy and malignant breast tissues, monostatic radar-based technique, slotted antenna array, SAR.**

I. Introduction

EARLY DETECTION IS YOUR BEST PROTECTION is the philosophy that drives breast cancer screening programs. According to the American Cancer Society, an estimated 316,950 women in the United States will be diagnosed with breast cancer in 2025 and the global incidence rates are expected to surpass these statistics [1]. Mammography is the primary imaging modality for breast cancer detection; however, it relies on ionizing radiation. Alternative diagnostic methods encompass Magnetic Resonance Imaging (MRI), sonography, and Computed Tomography (CT) scans. Nonetheless, MRI incurs high costs, sonography yields images of lower resolution, and CT scans utilize ionizing radiation, rendering them inappropriate for frequent screening [2, 3]. Microwave Imaging (MWI) has gained attention as a potential complementary modality in breast tumor screening, particularly due to its low cost, non-ionizing nature, and ability to detect dielectric contrasts in tissue. While it is not intended to replace gold-standard imaging methods, it may serve as a useful adjunct in specific clinical
scenarios, such as interim monitoring, in resource-constrained environments, or in combination with conventional imaging to provide additional functional information [4-6].

In the literature, various antenna-based sensors have been explored for breast tumor detection. The detection of breast tumors using dipole array relies on variations in the response of the reflection coefficient as a critical metric in [7]. Flexible monopole antenna sensors have been implemented in [8], yet their functionality is restricted to identifying tumors larger than 5 mm in diameter. A quarter mode substrate integrated waveguide (QMSIW) based antenna sensor is utilized in [9] for detection of tumor in a heterogeneous breast phantom. In [10], malignant breast tissues are detected via S-parameter analysis utilizing meta surface antenna. A monopole and spiral antenna array with 16 elements is presented in [11] for sensing the dielectric property differences of breast tissues. In recent years, numerous studies have explored the use of microstrip patch antennas for microwave breast cancer detection due to their advantages such as low profile, ease of fabrication, conformability, and compatibility with biological tissues. In [12, 13], microstrip patch antenna was proposed for breast lesion detection, where, the study did not demonstrate significant variations in the antenna response between the healthy and tumor conditions. In [14], a square patch antenna was designed, but no analysis was performed regarding tumor

The associate editor coordinating the review of this manuscript and approving it for publication was Roberto S. Murphy (*Corresponding author: V. L. Bhavani Maddirala*).

This article is submitted on 07.03. 2025 "This work is supported by ANRF (SERB Power Grant) project No. SPG/2021/002829."

D. Chaturvedi is with Department of Electronics and Communication Engineering, Indian Institute of Information Technology, Pune, Maharashtra, India (e-mail: divya@iiitp.ac.in).

V. L. Bhavani Maddirala is with the Department of Electronics and Communication Engineering, SRM University-AP, Andhra Pradesh, India (e-mail: bhavani_maddirala@srmap.edu.in).

A. Kumar is with the Department of Electronics and Communication Engineering, Visvesvaraya National Institute of Technology, Nagpur, Maharashtra, India (arvindkumar@ece.vnit.ac.in).

position or size variations. A multi-slotted microstrip patch antenna in [15], the analysis was limited to simulations with no experimental validation.

This work proposes 1×4 antenna-array-sensor that offers a significant advantage in terms of its low profile, achieved through a single-layered, single-port structure for detection of malignant breast tissues. A preliminary version of this work featuring a 1×2 antenna array was presented in [16] The proposed configuration facilitates conformity due to its thin dielectric laminate layer of thickness 0.508 mm which offers the advantages of lightweight and easy installation. Moreover, it operates in the frequency range of 5.725-5.875 GHz to meet the requirement of ISM band [17]. To enhance gain and overall sensitivity, the antenna-array is used instead of single element. Additionally, it covers a substantial area of the breast, eliminating the need for a large number of individually fed antennas and mechanical motors to reposition antenna elements across the breast. In evaluating performance, the 4-elements array antenna is compared with 1- and 2-element array antennas with respect to gain, efficiency, and current density.

The remainder of this paper is organized as follows: Section II describes the design methodology and working principle of the proposed antenna-array sensor. Section III presents the simulation results and analysis of the sensor's performance, including parametric studies. Section IV discusses the SAR analysis and its implications for tissue characterization. Section V details the experimental setup, phantom preparation, and validation of the proposed sensor through measurements. Finally, Section VI concludes the paper with a summary of key findings and potential directions for future work.

II. Design and Principle of Operation

The antenna-array-sensor comprises 4-identical slotted microstrip patch antennas. Initially, a rectangular microstrip patch antenna has been designed to operate around 6.9 GHz. The dimensions of the antenna are calculated by using the standard numerical empirical equations [18]. To reduce the size of the antenna, four rectangular slots of length l_s and width w_s are carved at a distance of a from the edge of the patch, as depicted in Fig. 1(a). The insertion of slots maintains the same characteristics of the dominant mode TM_{10}. Thus, after introducing the slot of length l_s, the operating frequency of dominant mode shifts downward, and it resonates at 5.8 GHz. This occurs because the introduction of slots increases the surface current path on the patch, effectively extending the electrical length of the antenna without increasing its physical dimensions. As a result, the antenna resonates at a lower frequency, allowing 35% reduction in the size of the antenna. The size of each antenna-element is $0.4\lambda_g \times 0.4\lambda_g$ whereas the overall size of the antenna-array including feeding network is ($L_T \times W_T$) $0.96\ \lambda_g \times 2.5\lambda_g$, as illustrated in Fig. 1(b). The comparison of the reflection coefficient (S_{11}) response for the proposed antenna, including single-element configurations without and with slots, as well as two-element and four-element array with slots is illustrated in Fig. 2.

A 1:4 equal power divider is employed to feed each antenna element in a corporate feeding network. In this method, firstly a 1:2 power divider is used to divide the power equally in two elements, where 50Ω characteristic impedance is divided into two 100Ω sections. By using a quarter wave transformer of length $0.25\lambda_g$ and impedance transformer of 70.7Ω, the impedance is transformed to 50Ω feedline. Further, two 1:2 power-divider networks are used to divide the power equally into 4-ports. The scalar electric field distribution of the 1-element, 2-elements and 4-elements array antenna has been displayed in Fig. 3. The field distribution is ensuring equal distribution of power to all four ports through a 4-way power divider with consistent magnitude and phase. We ensured equal electrical lengths for all feed lines, but slight phase shifts or variations in input impedance at each patch may still lead to unequal power absorption.

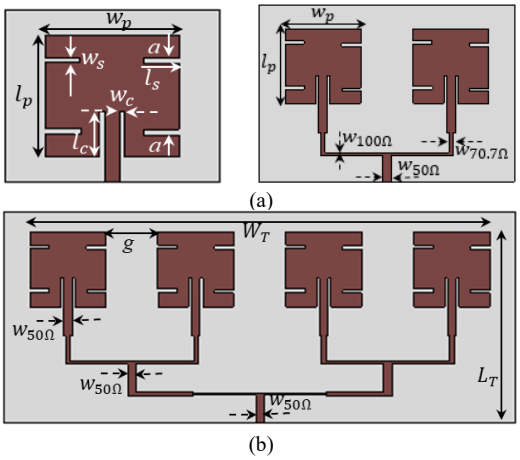

Fig. 1. (a) Schematic diagram of 1×2 array antenna and (b) Front view 1×4 array antenna, all dimensions (mm) $L_T = 38$, $W_T = 92$, $lp = 14.8$, $w_p = 15$, $l_s = 4$, $w_s = 0.6$, $l_c = 5.5$, $w_c = 0.6$, $a = 2.3$, $g = 10.4$, $w_{100\Omega} = 0.5$, $w_{50\Omega} = 1.6$, $w_{70.7\Omega} = 0.9$.

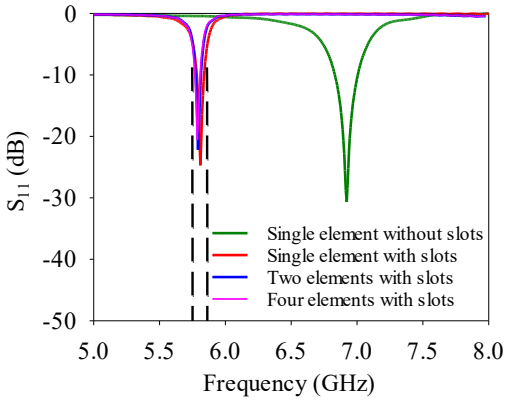

Fig. 2. S_{11} response of the proposed antenna: comparison between single-element configurations with and without slots, two- element and the four-element array with slots.

The S_{11} versus frequency response of the proposed antenna-sensor is examined by varying the length of the patch (l_p), length (l_s), width (w_s), and position *(a)* of the slots. Initially, l_s is varied from 3.5 to 4.5 mm with a step size of 0.5. It is clearly illustrated in Fig. 4(a) that as the length (l_s) of the slots increases, the resonant frequency shifts downward from 6.03 to 5.53 GHz. In the subsequent scenario, as shown in Fig. 4(b), the resonant frequency experienced a downward shift from 5.9 to 5.7 GHz when the width of the slot (w_s) is adjusted between 0.4 and 0.8 mm, with a step size of 0.2. In the next scenario, the position of

the slots (a) is varied from 2.2 to 2.4 mm from the edges of the patch with step size of 0.1. In this case, as the position of the slots varied, the resonant frequency experiences a downward shift from 5.84 to 5.76 as shown in Fig. 4(c). And lastly, the length of the patch (l_p) is varied from 14.6 to 14.8 mm with step size of 0.2, and it is observed that the resonant frequency experiences a downward shift from 5.85 to 5.76 as the patch length is increased as shown in Fig. 4(d). Based on the parametric analysis to obtain the desired resonant frequency 5.8 GHz with better impedance matching, the length, width and position of the slots are chosen as l_s = 4 mm, w_s = 0.6 mm, a = 2.3 mm and the length of the patch l_p = 14.8 mm.

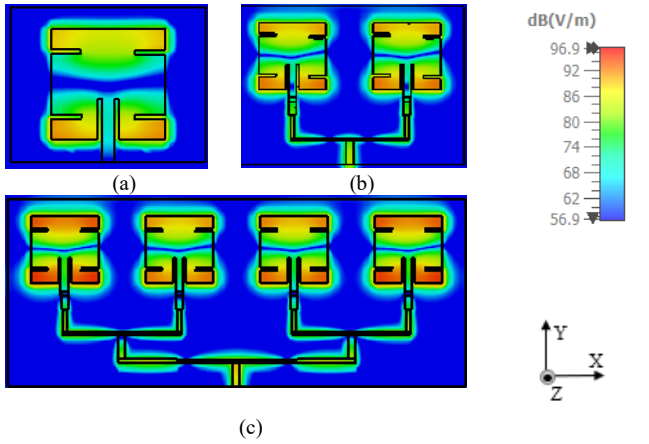

Fig. 3. Scalar E-field distribution (a) Single patch antenna, (b) 1×2 antenna-array and (c) 1×4 antenna-array.

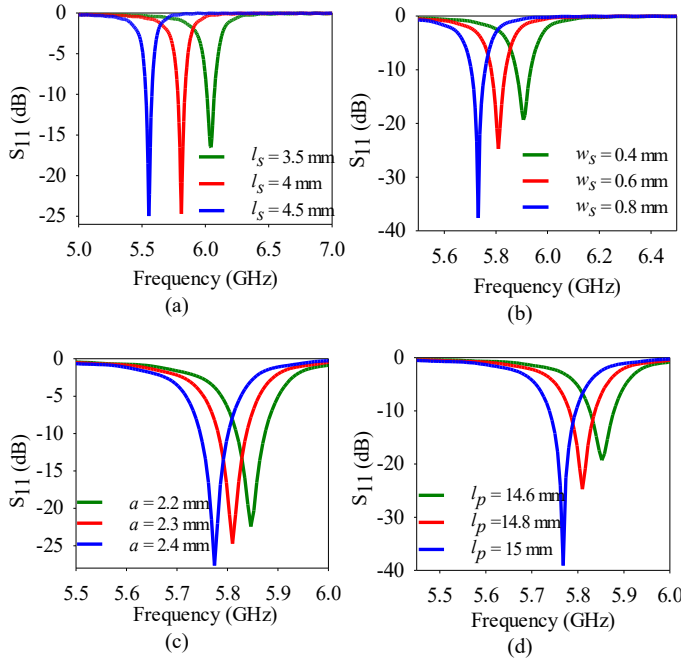

Fig. 4. S_{11} versus frequency response of the proposed antenna-sensor by varying (a) length (l_s) of the slots, (b) width (w_s) of the slots, (c) position *(a)* of the slots and (d) length of the patch (l_p).

The steps to design and analyze the proposed antenna-array sensor are summarized as follows.

Design Guidelines

1. *Design a rectangular patch antenna to operate at 6.9 GHz.*
2. *Introduce four identical rectangular slots on non-radiating edges at distance (a) from the edges of the patch.*
3. *Optimize the antenna/ slot-dimensions to operate it at 5.8 GHz.*
4. *Implement a 4-elements antenna-array maintaining equal distance between any two elements of 0.3λg.*
5. *Design a 1:4 equal power divider network with corporate feed using the quarter wave transformer technology.*
6. *Optimize the antenna-array to operate at 5.8 GHz.*
7. *Design an inhomogeneous female breast equivalent phantom in CST solver, further optimize the antenna-array to operate at 5.8 GHz.*
8. *Carry out simulation studies to observe the S_{11} against frequency response at different location/ different size of the tumor.*
9. *Manufacture the antenna-array sensors prototype and validate the simulation results with the experimental ones.*
10. *Illustrate the antenna-array response to evaluate the sensitivity performance in different scenarios of the tumors.*

III. Results and Discussion

To observe the competent sensing ability of the proposed design, it has been simulated on a multi-layered homogeneous female breast equivalent phantom model containing fat, skin, and tumor [19-22]. The phantom is designed using a hemispherical shape of different non-dispersive relative dielectric constant and conductivity. The simulations related to antenna-array design and optimization, along with its interaction with biological tissues through microwave energy, are conducted using a 3D electromagnetic wave solver, CST Microwave Studio 2022. The dielectric properties of different breast tissues are illustrated in Table I in terms of dielectric constant (ε_r), conductivity(σ) and mass density (ρ). In this context, the hemispherical breast phantom has a radius of 56 mm, with a 4 mm thickness for the skin layer, fat of radius 52 mm and a tumor of radius of 12.5 mm are opted. The simulation setup to examine variation in the sensor's response for healthy and malignant tissues is demonstrated in Fig. 5.

The depth of the tumor from the skin upper surface (i.e., k) is opted 10 mm. The antenna's stand-off distance from the phantom (i.e., h) is maintained at a constant value of 3 mm.

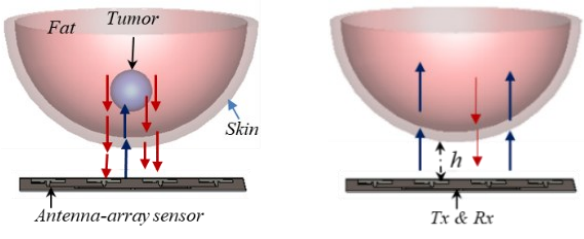

Fig. 5. Simulation setup: The proposed antenna-array in proximity of breast equivalent phantom with standoff distance h = 3 mm in presence of (a) Tumor and (b) Healthy tissues.

The penetration of electromagnetic (EM) waves through the various layers of breast tissue plays a vital role in identifying dielectric contrasts associated with abnormal tissue structures. The classification of a medium as a good dielectric or a good conductor is typically based on its loss tangent (tan δ), which quantifies the dielectric losses. The penetration depth (δ) of EM waves in a lossy dielectric medium is inversely related to the attenuation constant (α), and is given by the relation (δ) = 1/α (S/m). All these parameters are computed using standard empirical formulations as described in references [23, 24]. By calculating penetration depth, it is evident that the electromagnetic wave can effectively penetrate the skin layer to a depth of 10.5 mm, reach up to 27.5 mm within the fat, and penetrate the tumor to a depth of 8.8 mm as shown in Table I.

TABLE I
DIELECTRIC PROPERTIES OF BREAST TISSUES AT 5.8 GHZ [19-23]

	Brest tissues: properties	Fat	Skin	Tumor
1	Conductivity σ (S/m)	0.42	3.72	5.8
2	Dielectric constant (ε_r)	4.5	35.3	60
3	Density (ρ)	980	1010	1100
4	Attenuation Constant (α) Np/m	37	97	114
5	Skin depth (δ) in mm	27.5	10.5	8.8
6	Loss tangent (tan δ)	0.28	0.32	0.29

The performance of the 4-elements array antenna in free space, and in proximity of the breast phantom can be observed in Fig. 6(a). In proximity to the healthy tissues, the antenna resonates around 5.82 GHz. While in presence of tumor, the frequency is shifting down slightly, resonates around 5.81 GHz. Hence, the notable differences in frequency responses among three distinct media aid in determining the presence of malignant tissues. The radiation characteristics of the proposed antenna sensor have been assessed in terms of gain, efficiency, and 2D radiation pattern in free space, as well as in the presence of the phantom. The peak gain of the antenna is obtained as 11.9 dBi in free space, which decreases to 2.1 dBi in the presence of the phantom. Correspondingly, the radiation efficiency at the operating frequency is 90% in free space and reduces to 32.5% when the phantom is introduced as shown in Fig. 6(b). The antenna exhibits a directional radiation pattern, attributed to its array configuration, with the main lobe directed in the broadside direction. The cross-polarization levels are approximately 20 dB lower than the co-polarization levels in both principal planes (ϕ = 0° and ϕ = 90°), as illustrated in Fig. 7.

The performance of sensor is examined in different scenarios. First, the simulated S_{11} response has been observed at different locations of tumor by keeping tumor radius fixed (r = 10 mm). The location of the tumor is opted of L, L_1, L_2, L_3, L_4, where L_1/L_3 are 20 mm away from L while L_2/L_4 are 40 mm away from L in both direction of X-axis, respectively. It is clear from Fig. 8 (a) that by moving the antenna-sensor away from the center of breast towards ±X-axis, the operating frequency shifts higher side. The S_{11} response is the same for L_1 or L_3 and L_2 or L_4 location due to the same off-center distance. Moreover, to identify the stage of abnormality, the antenna-sensor's sensing ability has been observed with different sizes of tumor. In Fig. 8(b), it has been observed that there is an only minor change in return loss, however the resonant frequency is shifting downward consistently by increasing the tumor diameter (D). With increasing diameter of tumor in the range of 20–40 mm, the resonant frequency is shifting 5.82-5.807 GHz. Thus, a noticeable change can be observed in frequency response by varying the size and location of tumor.

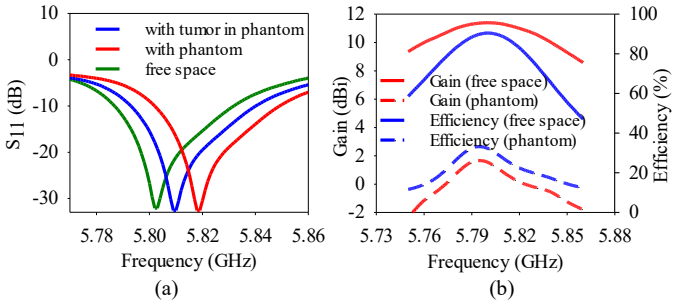

Fig. 6. (a) The reflection coefficient vs frequency in free space, healthy breast, and with tumor and (b) Simulated gain and efficiency plots in free space and in the presence of phantom.

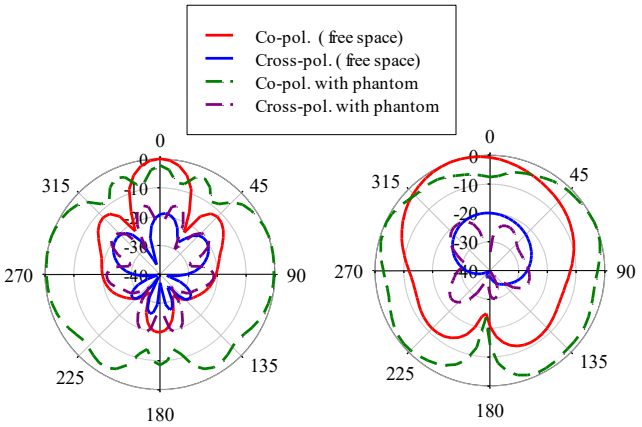

Fig. 7. 2D radiation pattern plots at 5.8 GHz in free space and in the presence of phantom at (a) ϕ = 0° and (b) ϕ = 90°.

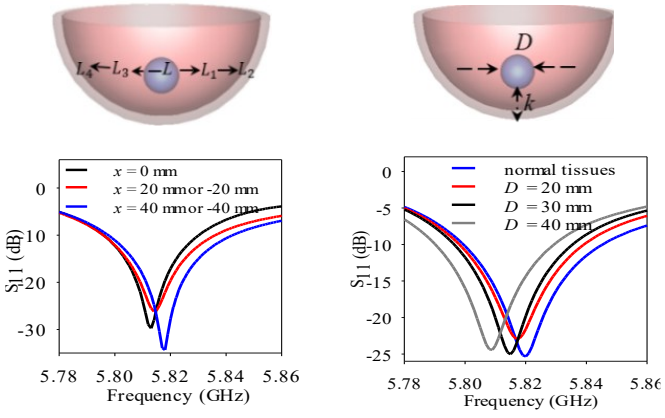

Fig. 8. S_{11} vs frequency response for (a) Different location of tumor and (b) Different size of the tumors.

IV. SAR Analysis

Another pivotal element to consider is the Specific Absorption Rate (SAR) when employing the antenna sensor for biomedical applications. The SAR measures the rate at which energy from an electromagnetic field is absorbed by biological tissues, typically expressed in watts per kilogram (W/kg) [25]. IEEE C95.1-1999 standard approved the safety regulations limits should be below 1.6W/kg for 1gm mass of the tissues. Thus, the antenna's input power is an important factor to create a safe and efficient product. Initially, the SAR is quantified for the healthy phantom, yielding a value of 1.48 W/kg for one gram of tissue at an input power of 25mW.

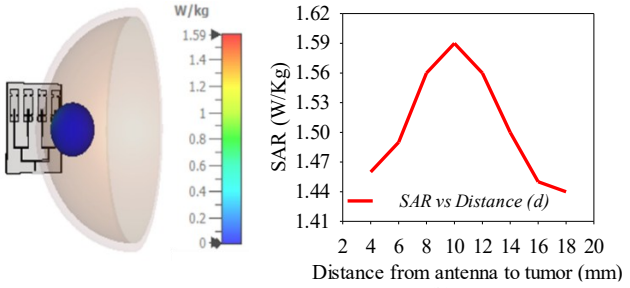

(a) (b)

Fig. 9. (a) Phantom showing Skin and fat layers with tumor of radius 12.5 mm and (b) Variation of SAR concerning distance of tumor from antenna.

Subsequently, a tumor of radius 12.5 mm is incorporated into the healthy phantom, and SAR is monitored in relation to the distance (d) of the tumor from the antenna [9]. From the analysis, it is evident that the SAR increases as the distance between the antenna and the tumor increases, reaching a maximum value of 1.59 W/kg at a distance of 10 mm, as depicted in Fig. 9(a). Beyond this point, with further increase in distance, the SAR gradually decreases, as shown in Fig. 9(b). This indicates that SAR analysis is crucial for distinguishing between healthy and cancerous tissues, providing valuable insights into tissue characteristics.

V. Experimental Results on Breast Phantom

The antenna-array is manufactured on RT Duroid 5880 substrate of ε_r = 2.2 and loss tangent 0.001. The fabricated prototype is shown in Fig. 10(a). To validate the simulated response, the phantom is prepared from common materials to replicate the dielectric properties of the real breast tissues. The breast phantom preparation procedure was adopted from the methodologies described in [26, 27]. To prepare the skin layer a vaseline solution is mixed with distilled water in the 4:1 proportion and stirred well to form a uniform solution. To prepare the fat equivalent, a mixture of olive and castor oil is mixed in the proportion of 4:1, that creates a solution quite close to fat tissues, as referred in. On the other hand, the tumor of different sizes are prepared with a mixture of wheat flour, corn flour, vaseline, few drops of distilled water, and olive oil as shown in Fig 10(b). To maintain the same stand-off distance as simulations, the fabricated prototype is first placed on the foam material covering the hemispherical bowl. The thickness of form is 3 mm and dielectric constant is 1.1. To observe the proposed antenna-array ability for sensing the tumor, S_{11} has been verified on the breast tissues mimicking phantom made of hemispherical bowl, as shown in Fig. 10(c). The return loss vs frequency response is repeated as similar to simulation by taking three different diameters (D = 20 mm, 30 mm, 40 mm) of the tumors.

The simulated and experimental response of proposed antenna-array in free space demonstrates a close agreement, as shown in Fig. 10(d). In Fig. 11(a), the experimental results clearly demonstrate that as the tumor size increases, the resonant frequency consistently shifts towards the lower end. From Fig. 11(b), it is evident that when the tumor's location offset is maintained, the frequency consistently shifts towards the higher side. Throughout the experiments, we maintained a consistent offset distance from the center (0, ± 20, ± 40 mm), mirroring the simulations. These experimental results confirm that the proposed array sensor is capable of detecting variations in tumor size and location, as evidenced by noticeable shifts in the S_{11} response.

The performance metrics outlined in Table II highlight several key advantages of the proposed 1×4 antenna-array sensor, which are essential for effective microwave-based breast tumor detection. First, it provides a significant gain enhancement (11.9 dBi) resulting in deeper and more efficient power penetration into breast tissues. Second, the array configuration enhances radiation directivity and efficiency, ensuring better coverage and field focusing. This focused radiation pattern contributes to a more concentrated and localized SAR distribution, which improves contrast between healthy and malignant tissues. These advantages collectively support the use of a 1×4 array for improved diagnostic performance. Also, the comparison of the proposed work with existing literature is presented in Table III.

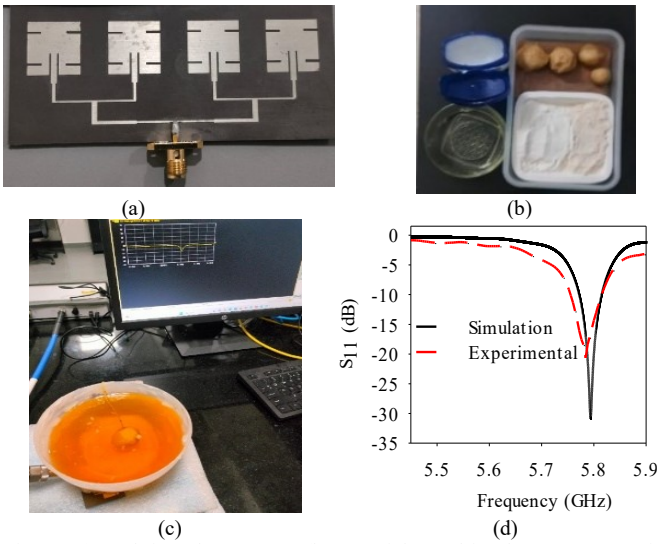

(a) (b) (c) (d)

Fig. 10. (a) Fabricated prototype, (b) materials used in phantom preparation along with different size of the tumors, (c) Antenna under test and (d) free space simulated and experimental S_{11} response for the proposed antenna-sensor.

It is important to note that the current breast phantom model is predominantly composed of skin and fat mimicking material and does not yet represent the complex heterogeneity found in real breast tissues, particularly in cases of high glandular density. This simplification, while useful for initial validation,

limits the clinical realism of the model. In future work, we plan to design heterogeneous phantoms incorporating distinct skin, fat, and glandular tissue layers to more accurately simulate various breast densities [19, 20].

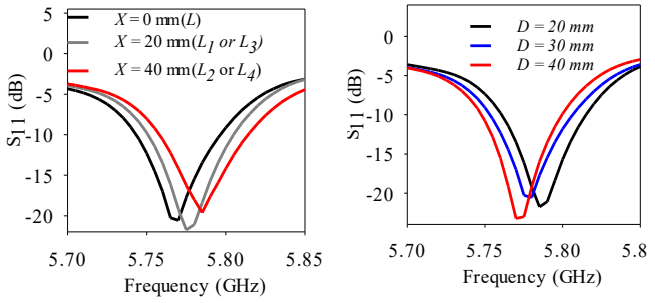

(a) (b)

Fig. 11. Measured S_{11} vs frequency response (a) for various location of tumors towards ($\pm X$ axis) and (b) for different size of tumors.

TABLE II
COMPARISON OF VARIOUS PARAMETERS FOR 1-ELEMENT, 2-ELEMENTS, 4-ELEMENTS ANTENNA

Parameters	1-element	2-element	4-element
3-dB beamwidth (free space)	93.5 deg	71.8 deg	67.1 deg
Current density (A/m^2)	1951	1200	890
Gain (free space)	4.4	7.30	11.9
Gain (on phantom)	1 dBi	1.25	2.1
Efficiency (free space)	90%	89%	90%
Efficiency (tumor)	21%	26.5%	32.5%

VI. CONCLUSION

This article presents the findings of a 4-element antenna array sensor operating within the 5.8 GHz ISM band. The antenna design takes inspiration from a standard rectangular patch antenna, achieving a 35% reduction in size by incorporating four rectangular slots along the non-radiating edges of the patch. To assess the performance, antenna arrays comprising 1-, 2-, and 4-elements are evaluated, ultimately selecting the 4-element array for its superior gain and lower SAR. The antenna-sensor's sensitivity is scrutinized in diverse scenarios, including different tumor locations and sizes. Simulated and measured observations reveal a noticeable shift in S_{11} vs frequency response corresponding to variations in tissue properties, distinguishing between healthy and malignant conditions. This variation in return loss and frequency response serves as a reliable indicator of tumor presence. The conducted SAR analysis is crucial for tumor localization, as SAR values exhibit variations depending on the tumor's proximity to the antenna.

Despite these promising results, the sensor currently relies solely on changes in S_{11}. Future work will focus on enhancing the realism and diagnostic relevance of the proposed sensor system. Planned improvements include the development of more complex breast phantoms incorporating distinct skin, fat, and glandular tissue layers to represent varying breast densities. Additional studies will also explore the sensor's performance in the presence of multiple tumors and benign structures such as fibroadenomas. Furthermore, the integration of image reconstruction algorithms and machine learning techniques will be investigated to support automated and robust interpretation of S_{11} responses, moving toward a more intelligent and clinically adaptable diagnostic platform.

ACKNOWLEDGEMENTS

I sincerely thank the ANRF for their financial support in sponsoring this research work. I also thank Ms. Shakshi Sharma for her assistance during the starting phase of this project.

REFERENCES

[1] M. Arnold et al., "Current and future burden of breast cancer: Global statistics for 2020 and 2040," Breast, vol. 66, pp. 15–23, Dec. 2022, doi: 10.1016/j.breast.2022.08.010.
[2] M. J. Yaffe and J. G. Mainprize, "Risk of radiation-induced breast cancer from mammographic screening," Radiology, vol. 258, no. 1, pp. 98–105, Jan. 2011, doi: 10.1148/radiol.10100655.
[3] A. M. Chiarelli et al., "Performance measures of magnetic resonance imaging plus mammography in the high-risk Ontario breast screening program," J. Nat. Cancer Inst., vol. 112, no. 2, pp. 136–144, Feb. 2020, doi: 10.1093/jnci/djz079.

TABLE III
COMPARISON OF PROPOSED WORK WITH EXISTING LITERATURE

Ref.	Band width (GHz)	Size of Sensors (mm) (L × W)	No. of sensors and Type	Peak Gain (dBi)	Analysis done for various tumor sizes and locations (Yes/No)
[7]	1.1 – 1.3	51 × 125	4 elements Dipole array	Not mentioned	Yes
[8]	2-8	50 ×50	1-element monopole	4	No
[9]	2.4–2.45	33 ×26	1- element QMSIW	3.71	Yes
[10]	2.56	90 ×90	1-element meta surface	Not mentioned	No
[11]	2-4	20 ×20 (single element)	4 × 4 Monopole and spiral	Not mentioned	No
[12]	2.45	57.5 ×115	2- element microstrip patch	5.38	No
[13]	5.72 – 5.82	12 ×12 (single element)	1- element microstrip patch	2.9	Yes
[14]	2.45	Not mentioned	Square Patch	Not mentioned	No
[15]	2.4 – 2.5	37.58 × 29.14	Slotted Patch	Not mentioned	No (only location analysis is done)
Prop. Sens.	5.7-5.8	38 × 92	4-element slotted patch	**11.9**	**Yes**

[4] E. C. Fear, P. M. Meaney, and M. A. Stuchly, "Microwaves for breast cancer detection?" IEEE Potentials, vol. 22, no. 1, pp. 12–18, 2003, doi: 10.1109/MP.2003.1180933.
[5] N. AlSawaftah, S. El-Abed, S. Dhou, and A. Zakaria, "Microwave imaging for early breast cancer detection: Current state, challenges, and future directions," J. Imag., vol. 8, no. 5, p. 123, Apr. 2022, doi: 10.3390/jimaging8050123.
[6] M. A. Aldhaeebi and T. S. Almoneef, "Dipole array sensor for microwave breast cancer detection," IEEE Access, vol. 11, pp. 91375–91384, 2023, doi: 10.1109/ACCESS.2023.3304694.
[7] D. M. Elsheakh, S. A. Alsherif, and A. R. Eldamak, "Textile monopole sensors for breast cancer detection," Telecommun. Syst., vol. 82, no. 3, pp. 363–379, Mar. 2023, doi: 10.1007/s11235-023-00990-x.
[8] M. V. L. Bhavani, D. Chaturvedi, T. Lanka, and A. Kumar, "Development of a QMSIW Antenna Sensor for Tumor Detection Utilizing a Hemispherical Multilayered Dielectric Breast-Shaped Phantom," IEEE Sens. J., vol. 24, no. 20, pp. 32080–32089, 2024, doi: 10.1109/JSEN.2024.3450990.
[9] D. Brizi, M. Conte, and A. Monorchio, "A Performance-Enhanced Antenna for Microwave Biomedical Applications by Using Metasurfaces," IEEE Trans. Antennas Propag., vol. 71, no. 4, pp. 3314–3323, 2023, doi: 10.1109/TAP.2023.3242414.
[10] H. Bahramiabarghouei, E. Porter, A. Santorelli, B. Gosselin, M. Popovic, and L. A. Rusch, "Flexible 16 antenna array for microwave breast cancer detection," IEEE Trans. Biomed. Eng., vol. 62, no. 10, pp. 2516–2525, Oct. 2015, doi: 10.1109/TBME.2015.2434956.
[11] H. V. Kumar and T. S. Nagaveni, "Design of Microstrip Patch Antenna To Detect Breast Cancer," *Online) Ictact J. Microelectron.*, vol. 1680, no. April, p. 1, 2020, doi: 10.21917/ijme.2020.0154.
[12] L. A. El Vadel, D. B. O. Konditi, and F. Moukanda Mbango, "A Miniaturized Antenna for Breast Cancer Detection at the 5.72-5.82 GHz ISM Band Based on the DGS Technique," *Prog. Electromagn. Res. B*, vol. 98, no. February, pp. 87–105, 2023, doi: 10.2528/pierb23011004..
[13] M. Elsaadi, H. Muhmed, M. A. Alraheem, H. Miftah, and O. Salah, "Square Patch Antenna for Breast Cancer Diagnosis at 2.45 GHz," *Circuits Syst.*, vol. 10, no. 04, pp. 45–53, 2019, doi: 10.4236/cs.2019.104004.
[14] M. S. Ahmed, Z. Ibrahim, M. M. Islam, M. Shahadat Islam Sumon, and A. K. M. Ehtesanul Islam, "Design and Analysis of Multi Slotted Micro-Strip Patch Antenna Operating in ISM Band for Breast Cancer Detection," *2023 26th Int. Conf. Comput. Inf. Technol. ICCIT 2023*, no. December, pp. 1–6, 2023, doi: 10.1109/ICCIT60459.2023.10441316.
[15] S. Sharma and D. Chaturvedi, "Slotted Rectangular Microstrip Patch Antenna for Breast Cancer Detection," *2023 Photonics Electromagn. Res. Symp. PIERS 2023 - Proc.*, pp. 2008–2013, 2023, doi: 10.1109/PIERS59004.2023.10221483.
[16] Federal Communications Commission (FCC), "*Code of Federal egulations Title 47, Part 18 – Industrial, Scientific, and Medical Equipment*," U.S. Government Publishing Office, Washington, DC, USA. [Online]. Available: https://www.ecfr.gov/current/title-47/chapter-I/subchapter-A/part-18.
[17] D. Gibbins, et al., "A comparison of a wide-slot and a stacked patch antenna for the purpose of breast cancer detection," *IEEE Trans. Ant. Propag.*, Vol. 58, pp. 665–674, 2010. doi: 10.1109/TAP.2009.2039296.
[18] M. Lazebnik et al., "A large-scale study of the ultrawideband microwave dielectric properties of normal, benign and malignant breast tissues obtained from cancer surgeries," Phys. Med. Biol., vol. 52, no. 20, pp. 6093–6115, Oct. 2007, doi: 10.1088/0031-9155/52/20/002.
[19] Cheng Y, Fu M. Dielectric properties for non-invasive detection of normal, benign, and malignant breast tissues using microwave theories. Thorac Cancer. 2018 Apr;9(4):459-465. doi: 10.1111/1759-7714.12605. Epub 2018 Feb 21. PMID: 29465782; PMCID: PMC5879051.
[20] S. Gabriel, R. W. Lau, and C. Gabriel, "The dielectric properties of biological tissues: II. measurements in the frequency range 10 Hz to 20 GHz," Phys. Med. Biol., vol. 41, no. 11, pp. 2251–2269, Nov. 1996. DOI 10.1088/0031-9155/41/11/002.
[21] N. Uncu and E. A. Aydin, "The effects of dielectric values, breast and tumor size on the detection of breast tumor," Tehni˘cki Glasnik, vol. 13, no. 3, pp. 197–203, Sep. 2019, doi: 10.31803/tg-20190226095826.
[22] M. N. Sadiku, Principles of Electromagnetics, 1st ed. London, U.K.: Oxford Univ. Press, 2015.
[23] C. A. Balanis, Advanced Engineering Electromagnetics. Hoboken, NJ, USA: Wiley, 2012.
[24] S. Subramanian, B. Sundarambal, and D. Nirmal, "Investigation on simulation-based specific absorption rate in ultra-wideband antenna for breast cancer detection," IEEE Sensors J., vol. 18, no. 24, pp. 10002–10009, Dec. 2018, doi: 10.1109/JSEN.2018.2875621.
[25] M. Bah, J. Hong, and D. Jamro, "Study of breast tissues dielectric properties in UWB range for microwave breast cancer imaging," *in Proc. Int. Conf. Comput. Inf. Syst*. Ind. Appl., vol. 18, 2015, pp. 473–475, doi: 10.2991/cisia-15.2015.129.
[26] K. E. Michaelsen, V. Krishnaswamy, A. Shenoy, E. Jor- dan, B. Pogue, and K. D. Paulsen, "Anthropomorphic breast phantoms with physiological water, lipid, and hemoglobin content for near-infrared spectral tomography," *J. biomed. optics*, vol. 19, no. 2, p. 026012, 2014. DOI: 10.1117/1.JBO.19.2.026012

Divya Chaturvedi (Senior Member, IEEE) received the B.Tech. degree in electronics and communication engineering from Uttar Pradesh Technical University, Lucknow, India, in 2011, and the M.Tech. degree in electronics engineering from Pondicherry Central University, Puducherry, India, in 2015, and the Ph.D. degree in substrate-integrated waveguide-based cavity-backed antenna from the National Institute of Technology, Tiruchirappalli, India, in 2019. Currently, she is working as an Assistant Professor at the Department of Electronics and Communication Engineering, IIIT Pune, Pune, Maharashtra, India.

M. V. L. Bhavani (Student Member, IEEE) received the B.Tech. degree in electronics and communication engineering and the M.Tech. degree in electronics engineering from Jawaharlal Nehru Technological University, Kakinada, India, in 2010 and 2012, respectively. She is currently pursuing the Ph.D. degree with the Department of Electronics and Communication Engineering, SRM University-AP, Amaravati, India.

Arvind Kumar (Senior Member IEEE) currently holds the position of Assistant Professor in the Department of ECE at VNIT Nagpur, India. Prior to this, he served as an Assistant Professor at VIT Vellore. He earned his Ph.D. in Microwave and RF in the Department of ECE at NIT Trichy, India, in 2019. In 2025 he was awarded young faculty research fellowship award by Ministry of Electronics & Information Technology, GoI. He was awarded the prestigious 'Scientific High-Level Visiting Fellowship' by the Government of France, enabling him to serve as a short-term visiting researcher at the University of Rennes-IETR.